Antimony modification of VOx/TiO2 NH3-SCR catalysts and the effect of thermal aging

Journal of Catalysis 450 (2025) 116303

Contents lists available at ScienceDirect

Journal of Catalysis

journal homepage: www.elsevier.com/locate/jcat

Research article

Antimony modification of VO_x/TiO_2 NH_3-SCR catalysts and the effect of thermal aging

Alexander Nellessen [a,b], Roberta Villamaina [c], Andreas Schaefer [a], Agnes Raj [c], Andrew Newman [c], Anna Martinelli [a], Per-Anders Carlsson [a,b,*]

[a] Department of Chemistry and Chemical Engineering, Chalmers University of Technology, Gothenburg, Sweden
[b] Competence Centre for Catalysis, Chalmers University of Technology, Gothenburg, Sweden
[c] Johnson Matthey Technology Centre, Blounts Court, Sonning Common, Reading, RG4 9NH, UK

ARTICLE INFO

Keywords:
NH_3-SCR
VO_x
Vanadium oxide
Antimony oxide
Aging

ABSTRACT

Titanium oxide supported vanadium oxide (VO_x/TiO_2) remains an important material for catalytic reduction of NO_x emissions, but to address future air pollution scenarios, its thermal stability must be improved without sacrificing its catalytic SCR activity. In this study, antimony oxide modified VO_x/TiO_2 catalysts were prepared *via* incipient wetness impregnation and investigated both in fresh state and after thermal stress at 580 °C in static air for 100 h, reflecting a common aging protocol in automotive applications. Characterization of the fresh and aged catalysts was performed by nitrogen physisorption, ammonia temperature-programmed desorption, Raman and *in situ* infrared spectroscopy and compared with the bare TiO_2 support and an unmodified VO_x/TiO_2 catalyst as references. The addition of antimony oxide stabilizes the anatase TiO_2 phase and shows an inherent standard SCR activity even in the absence of vanadium. The modification of VO_x/TiO_2 catalysts by antimony oxide reveal an improved SCR performance after aging despite the formation of V_2O_5 and rutile at a high V loading. This improvement may be related to enhanced redox properties that are influenced by the V/Sb molar ratio, with the catalyst having a molar V/Sb ratio of 1.2 showing particularly notable activity after aging. Variations in the impregnation sequence have shown that co-impregnation of both components in fresh state is the most favorable synthesis route in terms of standard SCR activity, although the catalytic properties converge after aging. Further, the modification with antimony oxide resulted in a significantly reduced N_2O formation, indicating improved selectivity toward the desired reaction.

1. Introduction

The awareness of the environmental impact of NO_x gases (NO and NO_2) originating from combustion processes, along with the introduction of legislative emission standards, has initiated the development of suitable technologies to meet the defined requirements. The selective catalytic reduction (SCR) of the NO_x gases with ammonia (NH_3) is the most common post-treatment method currently employed. The main reaction in this process is the reduction of NO_x gases with NH_3 in presence of oxygen, the so-called standard SCR reaction, subsequently forming nitrogen and water as shown in Eq. (1). For the application in mobile sources, a urea solution is used as ammonia source, decomposing to NH_3 and CO_2 when injected into the exhaust gas stream.

$$4NO + 4NH_3 + O_2 \rightarrow 4N_2 + 6H_2O \quad (1)$$

Vanadium oxide-based catalysts (VO_x/TiO_2) are commonly used in urea-based SCR systems as they have relatively low material costs, are resistant to sulfuric compounds, and show low formation of N_2O [1,2]. The respective loading of the catalytic active material is a crucial aspect for the activity and thermal stability of V-based SCR catalysts. Although a low V loading is beneficial for thermal stability, a high loading is generally associated with a higher SCR activity [3]. Depending on the loading, the vanadium oxide species are present in the form of monomers, polymers, or V_2O_5 crystallites. Polymeric VO_x species have shown the highest activity, which is associated with the so-called "coupling effect" where the interacting adjacent VO_x species shorten the regeneration time of the redox sites, thus resulting in an overall lower energy barrier of the catalytic cycle [4]. VO_x-based SCR catalysts currently used in industry, contain about 2 wt% of vanadium to achieve a high ratio of polymeric VO_x while minimizing undesired side reactions, e.g. the oxidation of SO_2 to SO_3, which can convert to sulfuric acid (H_2SO_4) in the presence of moisture [1,5,6].

* Corresponding author at: Department of Chemistry and Chemical Engineering, Chalmers University of Technology, Gothenburg, Sweden.
E-mail address: per-anders.carlsson@chalmers.se (P.-A. Carlsson).

https://doi.org/10.1016/j.jcat.2025.116303
Received 10 April 2025; Received in revised form 25 June 2025; Accepted 25 June 2025
Available online 18 July 2025

However, the application in mobile sources demand efficient and durable catalysts that have to fulfill specific requirements. The ideal SCR catalyst must function satisfactorily in a broad temperature window, with sufficient activity at low temperatures during cold starts, while also being stable at higher temperatures when engine loads are high [3]. Certain drawbacks of VO_x-based catalysts are the narrow temperature operating window of 300–400 °C, while exhaust temperatures can vary from 150 °C to 650 °C [3]. Another critical aspect is the potential formation and release of hazardous V_2O_5 [7], due to the relatively low Tammann temperature of bulk V_2O_5 (209 °C) [8]. This behavior was encountered in engine-based volatility tests with the release of small amounts of vanadium started from 500 °C under SCR conditions [9].

To meet these challenges, catalyst development focused on stabilizing the support, preventing the formation of V_2O_5, and improving the redox properties of the active phase by introduction of different additives [10]. The implementation of tungsten (W) modifier has been shown to promote the structural and thermal stability of the VO_x species while also extending the SCR activity temperature window towards higher temperatures [11]. Silicon (Si) has proven to maintain the stability of the TiO_2 support as it decelerates the sintering process [9, 12–15]. As the inclusion of W and Si has been extensively studied, current catalyst formulations can be considered to be almost mature. This motivates the search for new ways of structural improvement of VO_x/TiO_2 catalysts to improve the catalyst technology. Recently, the addition of antimony, cerium or niobium oxides have been proposed to be promising in order to meet the fore-mentioned challenges, such as improving low-temperature activity and thermal stability as well as resistance to H_2O and SO_2 [16–19]. While the synergistic impact of antimony has been studied in combination with tungsten [20], niobium [16], or cerium [21–24], only a few studies have been focused exclusively on the effect of antimony [16,25]. These studies, however, lack the analysis of the effect of thermal stress or aging.

The present work reports on the modification of VO_x/TiO_2 catalysts with antimony focusing on the physico-chemical and catalytic properties before and after thermal stress. Catalysts with industrially relevant vanadium loadings (1.5 to 3.5 wt%) were prepared, analyzed and compared with references. In addition, the influence of the impregnation sequence, i.e. co-impregnation or sequential impregnation of V and Sb, was investigated. The surface properties of fresh and thermally treated catalysts have been characterized with several techniques to correlate the surface area, crystallite size, and acidity with the catalyst structure. Specifically, *in situ* infrared spectroscopy was used to monitor surface species upon adsorption of NH_3 or NO, which are two common probe molecules that, one the one hand, provide essential information about surface sites and, on the other hand, are relevant for the SCR reaction.

2. Materials and methods

2.1. Catalyst preparation and characterization

The samples were prepared by incipient wetness impregnation of DT-51D TiO_2 powder (99 wt% anatase, Tronox plc) using ($VO(C_2O_4)$, GfE GmbH) and antimony(III) acetate solution ($Sb(CH_3CO_2)_3$, Sigma-Aldrich) as precursors. After impregnation, the powder samples were calcined in stationary air at 500 °C for one hour, referred to as 'fresh' samples. For the preparation of the sequential impregnated catalysts, the samples were calcined under the same conditions in between the precursor addition. In consideration of the fluctuating exhaust gas temperature in mobile sources between ambient and maximum temperatures, the combined effect of temperature over an extended period of time was tested. An accelerated aging protocol may include engine testing or an atmosphere-controlled lab furnace, aiming to test the catalysts under more realistic conditions (e.g. presence of water vapor or contaminants). However, those protocols are impractical for rapid screening tests. In this study, thermal aging was performed by exposing a portion of the fresh samples at 580 °C for 100 h in stationary air, correlating to a common operation situation the average conditions under operation. The resulting samples are labeled as 'aged'. An overview of the prepared samples with the targeted composition and physico-chemical properties is given in Table S.1.

The Brunauer–Emmett–Teller (BET) model was used to determine the specific surface area (SSA). To that end, nitrogen physisorption was measured at −196 °C with a Micromeritics Tristar 3000 instrument using approximately 200 mg of sample. Prior to the measurements, the samples were dried at 250 °C in a nitrogen flow for 6 h.

Temperature-programmed desorption (TPD) experiments with ammonia (NH_3) were conducted with a Sensys DSC calorimeter from Setaram. The outlet gases from the calorimeter were monitored by mass spectrometry (Hiden HPR 20 QUI MS). About 50 mg of the sample was pretreated in 10% O_2 at 500 °C for 30 min and cooled down to 100 °C in Argon atmosphere. 2000 ppm NH_3 was introduced for 2 h followed by purging with Argon until the NH_3 signal vanished. For the TPD experiment, the desorbed NH_3 signal (m/z = 17) was measured continuously while the temperature was increased from 100 °C up to 700 °C (at a rate of 5 °C/min) and kept constant at 700 °C for 30 min. The NH_3 uptake was determined by subtraction of the baseline and integration of the TPD profile. It should be noted that a potential source of error in the measurements are variations of the sample mass (±1 mg), which translates to an error of ±3% in the determined NH_3 uptake.

The crystallinity of the samples was analyzed with powder X-ray diffraction (XRD) on a Bruker AXS D8 Discover diffractometer equipped with monochromatic Cu-Kα radiation source (0.15406 nm) operating at 40 kV and 40 mA. The diffractograms were recorded under ambient conditions in the 2θ range from 10° to 80°, with incremental steps of 0.022° with a dwell time of 1 s. The TiO_2 anatase crystallite size was determined by adopting the Scherrer equation for the signal at the angle of 25°.

Raman spectroscopy was performed with an InVia Reflex spectrometer from Renishaw in the back scattering mode using a high power near-infrared diode laser (λ = 532 nm) as excitation source. The spectra were recorded under ambient conditions collecting 20 accumulations for 10 s each and using a laser power of 0.6 mW (measured along the optical path before the objective) to prevent any dehydration of the VO_x particles as a consequence of local heating. A spectral resolution better than 2 cm^{-1} was achieved using a grating with 2400 l/mm. The optical image of the selected spots (focused with a 50x Leica objective) was always checked before and after collecting the Raman spectra, to exclude any damage due to the laser illumination. The presented Raman spectra were baseline-subtracted using a linear background and normalized to the peak intensity of the feature at 639 cm^{-1}.

The *in situ* DRIFTS experiments were performed with a Bruker Vertex 70 spectrometer, which was equipped with a high-temperature stainless steel reaction cell (Harrick Praying Mantis™ High Temperature Reaction Chamber) with CaF_2 windows and a nitrogen cooled MCT detector. The temperature of the sample holder was controlled by a PID regulator (Eurotherm) and measured using a thermocouple (type K). Another thermocouple was placed within the sample bed to obtain the bed temperature. The feed to the reaction cell was controlled *via* individual mass flow controllers (Bronkhorst), with a total flow of 100 mL min^{-1} in all experiments. Only the particle size fraction of 40-80 µm of the sample powder was used. Prior to the experiment the samples were pretreated at a sample bed temperature of 290 °C with 10 vol% O_2 in Ar for 30 min and then cooled in Ar to the desired temperature, collecting a background spectrum. The experiments were performed by introducing a flow of 500 ppm NH_3 or NO to the reaction cell. The NH_3 adsorption was performed at 80 °C in order to avoid any potential interference with traces of co-adsorbed water. The region between 950–4100 cm^{-1} was recorded with a spectral resolution of 4 cm^{-1}. The peak decomposition was performed with the IGOR Pro 8 (wavemetrics) data fitting routine using a Levenberg–Marquardt algorithm. The spectra were fitted by several Voigt profiles with the

same shape parameter, which is defined as the ratio of Lorentzian and Gaussian widths ($\sqrt{\ln 2} \cdot (W_L/W_G)$), and the peak position were matched, based on the time-resolved spectra (details are specified in Ref. [26]). Prior to the fitting procedure, the spectrum was aligned with a spline and subtracted. In order to compare the decomposition of each sample before and after aging, the peak positions were fixed with a constraint of $\pm 0.5\,cm^{-1}$ while the intensity and width of the peaks were set free to vary.

The NH_3-SCR activity measurements and monitoring the N_2O formation were carried out in a vertical fixed-bed stainless steel flow-reactor. The synthetic feed gas was composed from high purity gases using a set of mass flow controllers with a top to bottom flow. The effluent gas stream including NO, NH_3, NO_2 and N_2O was analyzed continuously by on-line gas phase Fourier transform infrared (FTIR) spectrometer (MKS). About 0.3 g of pelletized powder (250–300 µm) was used for each sample. In order to represent the operation of common SCR converter in heavy-duty vehicles, the reaction conditions were controlled as follows: 500 ppm NO, 525 ppm NH_3, 300 ppm CO, 3% CO_2, 10% O_2, 5 vol% H_2O and N_2 balance with a gas hourly space velocity of 60,000 h^{-1}. The sample was exposed to the reaction mixture at 175 °C until stable and the temperature was then increased stepwise to 200, 225, 250, 300, 350, 400 and 450 °C with 30–40 min at each temperature. The FT-IR spectra were collected after the SCR reaction reached a steady state, and the NO_x conversion was calculated as follows:

$$NO_x \text{ conversion} = \frac{[NO_x]_{in} - [NO_x]_{out}}{[NO_x]_{in}} \cdot 100\% \quad (2)$$

Using the NO_x conversion data collected in the kinetically controlled regime, the apparent activation energy (E_{app}) was estimated *via* Arrhenius plots where ln(NO_x conversion) was plotted against 1/T. From the slope (m), the apparent activation energy was calculated as $E_{app} = -m \cdot R$ with $R = 8.3145$ J/(mol K).

3. Results and discussion

3.1. Impact of antimony on TiO_2

A comparison of the specific surface area (SSA) and crystallite size for the bare (TiO_2) and modified support (Sb/TiO_2) reveals that antimony has a stabilizing impact on the anatase phase. After the aging procedure, the surface area of the bare support decreases by about 46% (from 88 to 47 $m^2\,g^{-1}$). This loss is mainly due to particle growth of the anatase phase [27], as confirmed by XRD analysis which reveals an increase of the particle size by 24% (from 196 to 257 Å). In contrast, with the addition of antimony, the surface area is preserved for the modified support (Sb/TiO_2) showing a minor loss of 5% (from 76 to 72 $m^2\,g^{-1}$) and a nearly unaffected particle size after aging (from 197 to 204 Å), proving a stabilizing effect of antimony on TiO_2. The respective XRD diffractogram (SI, Fig. S1) is dominated by TiO_2 anatase signatures, whereas no signatures related to antimony-oxides or -titanates were observed, indicating a high dispersion of antimony oxide particles.

The sample surface and the interaction with ammonia, a key reactant in the SCR reaction, were further studied *via* ammonia temperature-programmed desorption experiments (TPD) and *in situ* DRIFTS upon adsorption of NH_3. The NH_3 uptake was determined based on integration of the TPD profiles (SI, Fig. S2). The comparison of the NH_3 uptake for the bare support before and after aging shows a similar trend as to the surface area, with a decrease of 44% (from 250 to 141 µmol g^{-1}). Upon modification with antimony, the NH_3 uptake is relatively low (80 µmol g^{-1}), indicating that antimony does not enhance the overall acidity nor provides additional acid sites. Notably, after the aging procedure, the NH_3 uptake is increased by 54% (to 123 µmol g^{-1}).

The DRIFT spectra in Fig. 1 show NH_3 ad-species by positive adsorption bands in the region between 1700 and 1100 cm^{-1} and provide information about Lewis and Brønsted acid sites. Negative features are

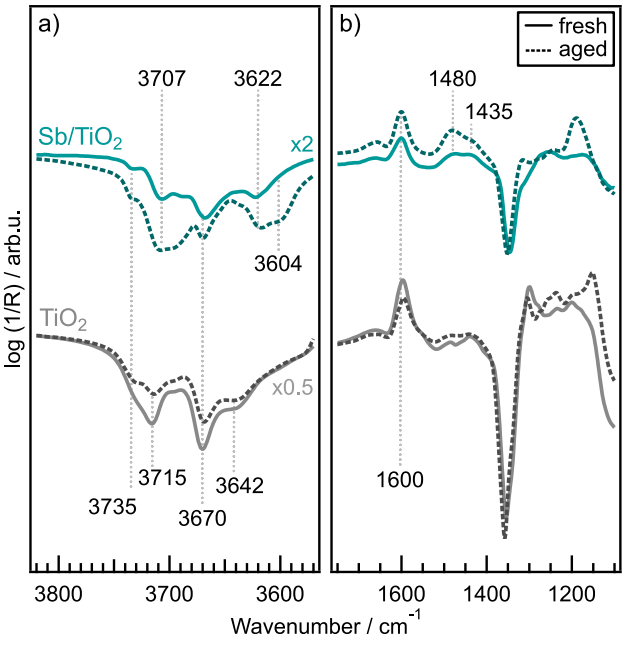

Fig. 1. DRIFT spectra of the bare and Sb-modified TiO_2 support before (solid line) and after (dashed line) aging for the NH_3 adsorption at 80 °C. (a) ν(O-H) region and (b) δ(N-H) deformation modes of ammonia. The OH bands were adjusted by factor *x* for a better visibility.

observed in the region 3800–3500 cm^{-1}, which result from suppressed O-H vibrations due to the coverage by ammonia coupled with the formation of NH_4^+. In addition, the negative band around 1360 cm^{-1} originates from hindered S=O stretching vibrations from surface sulfates as the support is prepared *via* the sulfate route [28–30].

The bare TiO_2 support exhibits a series of suppressed OH bands (Fig. 1a) that are related to isolated (3735, 3715 cm^{-1}) and bridged (3670, 3642 cm^{-1}) titania hydroxyl groups on different surface facets [27], while the adsorption bands in the N-H deformation region (Fig. 1b) (1700–1100 cm^{-1}) signify ammonia adsorption predominantly on Lewis acid sites (1600 cm^{-1}). Minor bands at 1470–1440 cm^{-1} origin from ammonium cations (NH_4^+) formed by the protonation of adsorbed ammonia, hence Brønsted acid sites are available on the bare support. As demonstrated in our earlier work [26], Brønsted acid sites can be differentiated by the N-H vibrations of the ammonium cation that is formed on isolated (1480 cm^{-1}) and bridged (1430 cm^{-1}) hydroxyl groups, thus declared as monomeric and polymeric Brønsted acid site. With the addition of antimony (Sb/TiO_2), the intensity of the suppressed OH signals is relatively low, suggesting that most of the TiO_2 sites are covered by antimony entities. The bands at 3670 and 3735 cm^{-1} are related to the OH groups of titania, while the bands at 3707 and 3624 cm^{-1} are suggested to origin from isolated Sb-OH and bridged OH groups, either Sb-(OH)-Ti or Sb-(OH)-Sb, as there are no such bands on the bare TiO_2 support. The ammonia adsorption bands reveal the adsorption mainly on Lewis acid sites (1600 cm^{-1}) along with weak bands of Brønsted acid sites (1480–1440 cm^{-1}). After the aging procedure, the OH bands intensify with the band at 3707 cm^{-1} as a new main band, and a shoulder around 3604 cm^{-1} is observed. The more intense band at 3707 cm^{-1} suggests that more isolated Sb-OH sites have formed throughout the aging process while revealing additional TiO_2 sites as the intensity of the bands at 3735 and 3670 cm^{-1} also increase. The presence of bridging OH groups is evident by the increased intensity of the bands at 3622–3604 cm^{-1} and are assigned to Sb-(OH)-Sb and Sb-(OH)-Ti. The N-H deformation modes exhibit that the intensity of both Lewis (1600 cm^{-1}) and the monomeric Brønsted acid sites (1480 cm^{-1}) increase. Thus, the *in situ* DRIFT spectra indicate that throughout thermal treatment, more

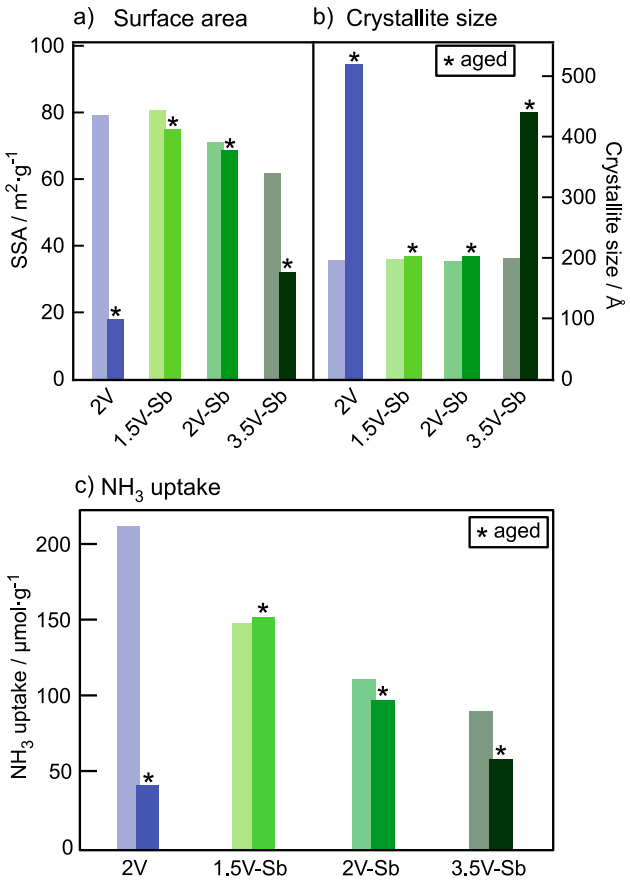

Fig. 2. Comparison of (a) specific surface area (SSA), (b) TiO_2-anatase crystallite size based on XRD and (c) NH_3 uptake based on NH_3-TPD measurements for the V-Sb catalysts with a different V loading as well as the reference catalyst (2V) before and after (*) aging.

isolated Sb-OH and Sb-(OH)-Ti groups are formed while additional TiO_2 sites are exposed. Those observations correlate with the findings of Eppler [31], suggesting the incorporation of antimony into titania, forming Sb-O-Ti bonds, below temperatures of 870 °C. The exposed additional TiO_2 may contribute to the observed higher NH_3 uptake after aging, due to the fact that titania has a higher inherent NH_3 adsorption energy than vanadium oxides [32,33].

In terms of the NH_3–SCR performance, the fresh modified support reveals a NO_x conversion of 26% at 300 °C and maximizing to 49% at 450 °C (SI, Fig. S3), proving an inherent SCR activity of antimony oxide. After aging, the NO_x conversion depletes and drops by about 20% for most temperatures.

3.2. Impact of antimony on VO_x species

In this section, the promotional effect of antimony on vanadium oxide catalysts is reported. Three catalysts were prepared with an increasing vanadium loading of 1.5, 2.0 and 3.5 wt% V, reflecting industrial relevant vanadium loadings in commercial catalysts [34,35], with a respective V/Sb molar ratio of 0.9, 1.2 and 2.1. The maximum vanadium loading of 3.5wt% was chosen as to avoid significant formation of V_2O_5. An unmodified catalyst with a vanadium loading of 2.0 wt% was used as a reference.

Fig. 2a compares the specific surface area of the catalysts before and after the aging procedure. In fresh state, the reference catalyst (V/Ti) exhibits a specific surface of 79 $m^2\,g^{-1}$, which decreases by 77% to 18 $m^2\,g^{-1}$. This significant loss is most likely related to the TiO_2 particle growth promoted by the presence of vanadium [3,26,27]. Concurrently, the crystallite size of the TiO_2-anatase signature significantly increases from 195 to 519 Å, as seen in Fig. 2b. The SSA of the modified catalysts in fresh state decreases from 81 to 62 $m^2\,g^{-1}$ as the vanadium loading increases. It is likely that a higher vanadium loading causes pore blocking [3,26]. After aging, the surface area of the 1.5V-Sb and 2V-Sb catalysts is slightly decreased (13% for 1.5V-Sb, -3% for 2V-Sb), in conformity with a maintained crystallite size. By contrast, with a loading of 3.5 wt%, a significant decrease of 57% in SSA from 62 to 32 $m^2\,g^{-1}$ is observed, along with a pronounced growth of crystallite size (from 199 to 440 Å).

The determined NH_3 uptake (Fig. 2c) of the reference catalyst is 213 µmol g^{-1} and significantly reduces to 42 µmol g^{-1} (−80%) after aging, which is attributed to a loss of surface area. With added antimony, the NH_3 uptake of the fresh modified catalysts is lower in fresh state (149, 112, and 81 µmol g^{-1}) indicating that antimony does not enhance the overall acidity or interaction with ammonia. However, as the vanadium loading increases, the determined NH_3 uptake decreases. In an earlier study [26], it was observed that a high SSA and NH_3 uptake were mainly attributed to the degree of uncovered titania. Further, it must be mentioned that SSA or NH_3 uptake are not considered to be the limiting parameters for the SCR activity under stationary conditions. The 1.5V-Sb catalyst reveals an increased NH_3 uptake after aging (149 to 153 µmol g^{-1}, +2%), following the same phenomena as for the modified support. As noted in the Experimental section, the determined value can deviate by ±3% due to potential variations of the sample mass. While 2V-Sb reveals a slight loss of −13% (112 to 98 µmol g^{-1}), the 3.5V-Sb catalysts reveals a significant decrease of −35% (91 to 59 µmol g^{-1}), in agreement with the results for SSA and crystallite size. To summarize, compared to the reference sample, all modified catalysts demonstrate a higher preservation of the NH_3 uptake throughout the aging procedure.

The results from the XRD and Raman measurements are shown in Fig. 3. XRD measurements were conducted to determine the crystallinity of the samples and observe the potential formation of crystallites due to aging. The X-ray diffractograms of all samples in fresh state show broad patterns of TiO_2-anatase. No patterns related to oxides of vanadium, antimony, or vanadates (e.g. $SbVO_4$) could be observed, suggesting a high dispersion of the compounds in an amorphous state or below the detectable level. After the aging procedure, the anatase signatures of the reference catalyst significantly increase (SI, Fig. S1), since vanadium accelerates the particle growth of TiO_2 [26,27]. Both the 1.5V-Sb and 2V-Sb catalysts underline the stabilizing effect of antimony on TiO_2 as neither significant changes in the signatures nor additional signatures occur. The 3.5V-Sb catalyst shows strong features of rutile TiO_2 and patterns of V_2O_5 indicating the formation of those compounds and a phase transformations throughout thermal treatment.

Raman spectroscopy was used to investigate the distribution of VO_x species on the catalyst surface and alterations after aging. The spectral region between 1050 and 700 cm^{-1} is characteristic of the fundamental vibrational modes of metal-oxo groups of VO_x species, while the region between 650 and 350 cm^{-1} is dominated by TiO_2 bands (SI, Fig. S4). The feature at 795 cm^{-1} is assigned to a second order vibration [36]. The modified catalysts with a vanadium loading of 1.5 and 2.0 wt% show a broad feature in the region of 900–930 cm^{-1}, which can be attributed the overlay of V-O-Ti vibrations (942 cm^{-1} [37]) and V-O-V vibrations (890 cm^{-1} [38,39]) related to polymeric VO_x species. The origin of the feature at 1000 cm^{-1} cannot be definitively explained. In our earlier study [26], features around 1019 cm^{-1} were observed for a vanadium loading close to or above monolayer coverage, and consequently relate to a high degree of polymerized VO_x. Due to the inevitable presence of moisture under ambient conditions, the vibrational features of isolated or monomeric V = O vibrations (around 1030 cm^{-1}) cannot be observed [26,38]. Consequently, the feature at 1000 cm^{-1} is considered to relate to highly polymerized VO_x. Therefore, the addition of antimony implies to have a structural effect on the formation of VO_x with a higher degree of polymerization, since no such feature is

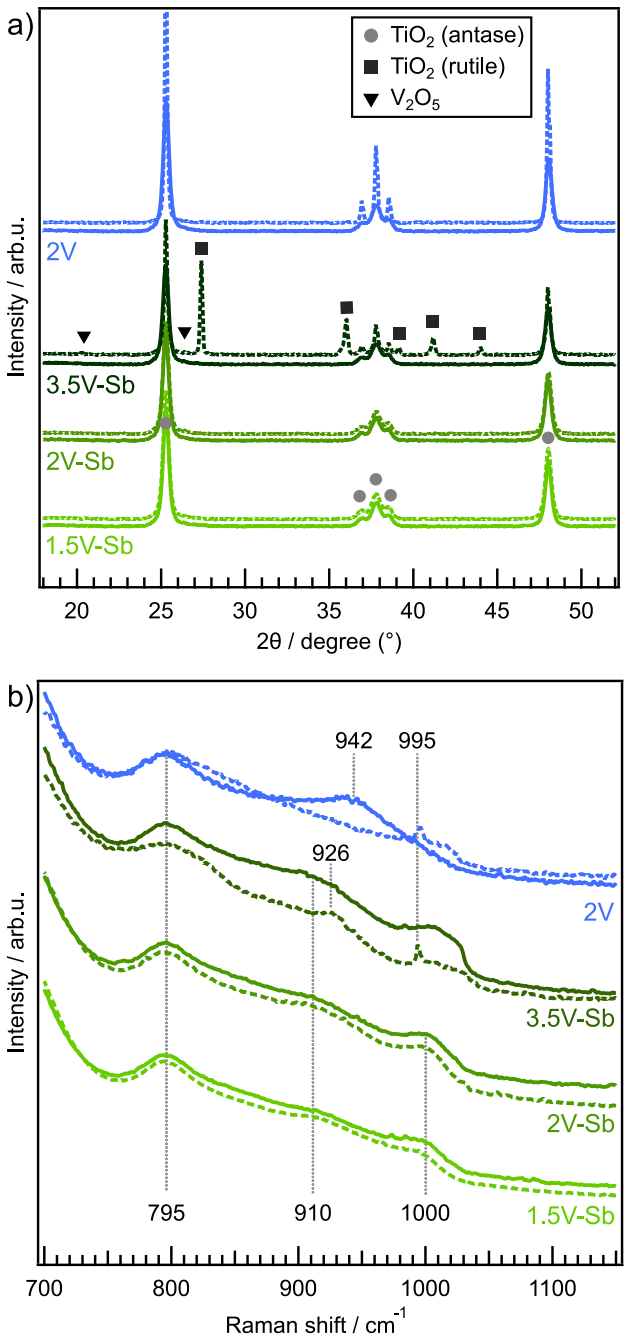

Fig. 3. (a) Background subtracted XRD patterns and (b) Raman spectra (λ = 532 nm) of the V-Sb catalyst with a different V loading before (solid line) and after (dashed line) aging under ambient conditions.

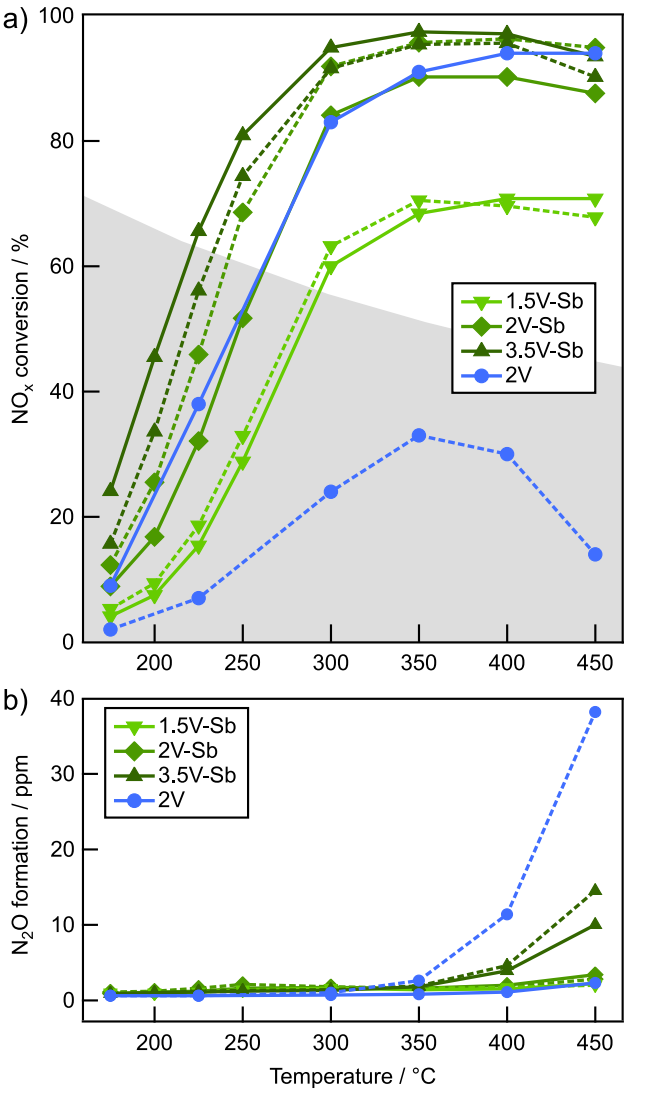

Fig. 4. (a) NO_x conversion and (b) N_2O formation of the V-Sb catalysts with a different loading and the reference catalysts (2V) before (solid line) and after (dashed line) aging. The shaded area shows the region where the reaction is kinetically controlled, see SI for mass transfer analysis. Reaction conditions: 525 ppm NH_3, 500 ppm NO, 300 ppm CO, 3% CO_2, 10% O_2, 5% H_2O in Ar/N_2 balance with a GHSV = 60,000 h^{-1}.

observed for the reference catalyst. The Raman spectra collected after the aging procedure do not show any shifts or additional features, indicating that the VO_x species are not affected by thermal stress of the aging procedure, which is in agreement with the results from XRD. By contrast, the unmodified catalyst reveals a sharp feature (995 cm^{-1}) which is related to crystalline V_2O_5 [38,39]. In addition to a feature for V_2O_5 (995 cm^{-1}) the aged catalyst with a vanadium loading of 3.5 wt% shows features related to rutile TiO_2 at lower Raman shifts (SI, Fig. S4), in agreement with X-ray diffraction.

Fig. 4 shows the steady-state NO_x conversion and N_2O formation as a function of temperature in the range of 175 to 450 °C for the modified catalysts and the reference before and after aging. The formation of NO_2 is not shown since it has not been detected at any temperature. The fresh reference catalyst (2V) reveals a steady increase of the NO_x conversion as a function of the temperature. At low temperatures (225 °C), a NO_x conversion of 38% is observed, then in the mid-temperature region (300–350 °C) it further increases to 83 and 91%, while the highest NO_x conversion of 94% is achieved in the high-temperature range (400–450 °C). After the aging procedure, the NO_x conversion is significantly lower at all temperatures with a maximum NO_x conversion of 33% at 350 °C. The decline in performance is attributed to the significant loss of surface area along with the formation of V_2O_5, which is detrimental to the desired reaction selectivity [26].

The modified catalyst with a vanadium loading of 2 wt% (2V-Sb) shows a performance similar to the reference catalyst at temperatures between 250 to 350 °C, while outside this range the NO_x conversion slightly drops with a deficit of maximum 6%. After the aging procedure, the NO_x conversion is improved across all tested temperatures, with a maximum of 96% at 300 and 400 °C. The 1.5V-Sb catalyst achieves an overall lower NO_x conversion given to lower amount of active material, reaching a maximum of 71% at 450 °C. After aging, the activity in the low- to mid-temperature regime slightly increases, while marginal

lower at temperatures above 400 °C. For the 3.5V-Sb sample the overall highest NO_x conversion across the samples in the low-temperature region and peaks at 97% at 350-400 °C then slightly falls off to 94% at 450 °C. After aging the activity is decreased by 6% on average.

The V/Sb molar ratio seems to be a critical factor for the thermal activation of SCR activity, as only the 2V-Sb catalyst (molar ratio 1.2 V/Sb) shows a significant increase in performance. It is generally accepted that the catalytic cycle in the SCR reaction involves acid sites activating NH_3, and redox sites regenerating the vanadium species in presence of oxygen [40,41]. The latter are considered to be the rate determining step [42,43]. As a consequence, the thermal treatment and interaction of Sb with V and in that specific ratio seems to enhance those redox properties. The calculation of the specific reaction rate (SI, Fig. S5) confirms those observations. When normalized to the amount of vanadium, the aged 2V-Sb catalysts shows the highest activity at low temperatures (225 °C) as well as at higher temperatures (300 °C) after the aging procedure. While with a higher V loading (3.5V-Sb) the low-temperature activity in fresh state is the highest compared to the other catalysts, although revealing a moderate performance at higher temperatures and after aging.

The apparent activation energy is rather similar for all catalysts (SI, Fig. S6), especially for the aged catalysts, giving no evidence for different operating SCR mechanisms for different catalysts. Although the Arrhenius plots are based on a few number of points, these results could indicate that the improved activity for NO reduction seen at low temperatures for antimony modified catalysts is not caused by lower barriers for redox processes. Instead, this is likely due to an increased availability of active surface oxygen species. For the fresh vanadium only (2V) and low loaded vanadium antimony (1.5V-Sb) catalysts a slight decrease in apparent activation energy can be seen upon aging, which may be due to formation of V-O-V/V-O-Sb species during the thermal treatment.

The N_2O formation over the fresh reference catalyst and the 1.5V-Sb and 2V-Sb catalysts is low, ranging from 0.8 to 3.4 ppm across all temperatures. In contrast, the 3.5V-Sb catalysts shows an elevated N_2O formation of 10 ppm at 450 °C, further increasing to 14.5 ppm after the aging procedure. The aged reference catalyst exhibits a maximum formation of 38.2 ppm at 450 °C. The enhanced N_2O formation is associated with the presence of crystalline V_2O_5 and/or highly polymerized VO_x species, which are known to promote side reactions [26] leading to N_2O production. The presence of V_2O_5 on 3.5V-Sb and 2 V was confirmed by both XRD and Raman spectroscopy, supporting its correlation with the observed trend.

The results show that the modification by antimony may not substantially promote the activity in fresh state, but significantly preserves the activity after thermal aging. Additionally, the N_2O formation at high temperatures is significantly lower in comparison to the unmodified catalysts.

The *in situ* DRIFT spectra recorded after exposing the sample to 500 ppm NH_3 (Fig. 5) show strong bands related to suppression of bridged Sb-(OH)-V hydroxyl groups (3624 cm^{-1}) on the 1.5V-Sb catalysts, alongside with suppression of isolated Sb-OH (3695 cm^{-1}) and vanadium hydroxyl (V-OH and V-(OH)-V around 3650 cm^{-1}) groups. After aging, the intensities of the vanadium hydroxyls and Sb-OH bands are increased while the intensity of the bridged Sb-(OH)-V groups decreases, suggesting segregation of vanadium and antimony on the surface throughout the aging process, resulting in isolated Sb-OH and more available sites of V-OH or V-(OH)-V. The 3.5V-Sb catalyst shows primarily features related to V-OH and V-(OH)-V sites. After aging, the overall intensity of the OH bands is decreased, consistent with the losses in the specific surface area and NH_3 uptake. In the N-H vibrational region (1800–1200 cm^{-1}), the catalyst with a low loading (1.5V-Sb) reveals two overlapping bands at around 1470 and 1435 cm^{-1}, reflecting the vibrations of NH_4^+ on isolated (1470 cm^{-1}) and bridged (1435 cm^{-1}) Brønsted acid sites. As the vanadium loading increases, the Brønsted acid sites shifts to 1435 cm^{-1} as main band, indicating

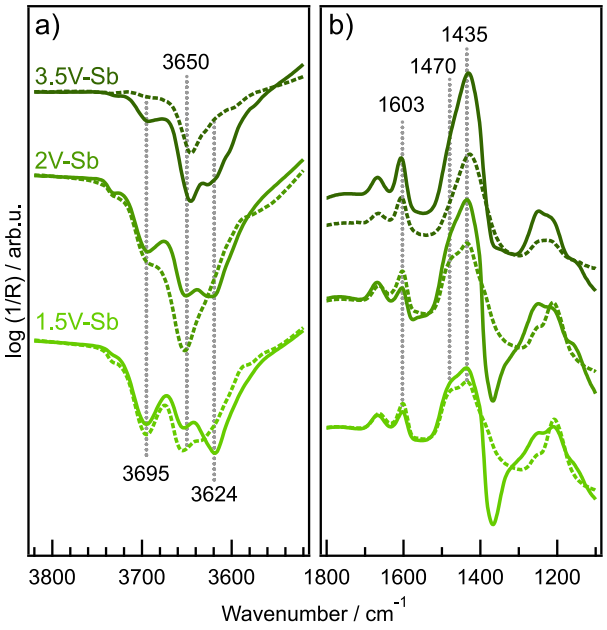

Fig. 5. DRIFT spectra of the V-Sb/TiO_2 catalyst with different V loading before (solid line) and after (dashed line) aging for the NH_3 adsorption at 80 °C. (a) ν(O-H) region and (b) δ(N-H) deformation modes of ammonia.

Table 1
Proposed band assignment of the OH groups (3700–3600 cm^{-1}) in this work and bands of adsorbed ammonia based on Ref. [26].

Position/cm^{-1}	Assignment	Vibration
3707–3695	terminal Sb-OH	ν(OH)
3624	bridging Sb-(OH)-V	ν(OH)
3622–3604	bridging Sb-(OH)-Sb/Sb-(OH)-Ti	ν(OH)
3650	terminal V-OH [26]	ν(OH)
3635	bridging V-(OH)-V [26]	ν(OH)
1470	monomeric Brønsted acid site [26]	δ_{as}(NH)
1433	polymeric Brønsted acid site [26]	δ_{as}(NH)
1606	polymeric Lewis acid site [26]	δ_{as}(NH)
1595	monomeric Lewis acid site [26]	δ_{as}(NH)

the formation of NH_4^+ predominantly on bridged OH sites. The absence of the band associated to surface sulfates (around 1360 cm^{-1}) also suggests a full coverage of the TiO_2 support. After the aging procedure, the Brønsted band intensity for the 1.5V-Sb catalyst is maintained while significantly affected with a high vanadium loading (3.5V-Sb). The adsorption bands of coordinatively bound ammonia (1603 cm^{-1}) on Lewis acid sites do not undergo any significant band shifts. Notably, the intensity after aging is increased for 1.5V-Sb and 2V-Sb, while decreased for 3.5V-Sb. An overview of the exemplified infrared bands and their assignment is given in Table 1. When comparing the DRIFT spectra with the activity data it seems that increased performance after aging is directly related to the increased intensity of the V-OH (3650–35 cm^{-1}) groups in 2V-Sb and 1.5V-Sb while only for 3.5V-Sb the intensity decreases coherently with the reduced NO_x conversion.

The adsorption of NO on TiO_2-supported metal oxides is commonly characterized by formation of surface nitrates and NO_2 in the wavenumber region of 1800–1200 cm^{-1}. The spectra for the NO adsorption (Fig. 6a) on the V-Sb/TiO_2 catalysts with a V loading of 1.5 and 2 wt% feature a main adsorption band around 1625 cm^{-1} which is associated to NO_2, followed by signals related bidentate nitrates (1578, 1235 cm^{-1}), while monodentate nitrates (~1510 cm^{-1}) are weakly represented in the spectra. Two other sets of broad bands located around 2190 and 1990 cm^{-1} arise from adsorbed nitrosonium (NO^+) and NO species (not shown for brevity, c.f. SI, Fig. S7). The catalyst with 3.5 V loading shows bridged nitrates as main species with the

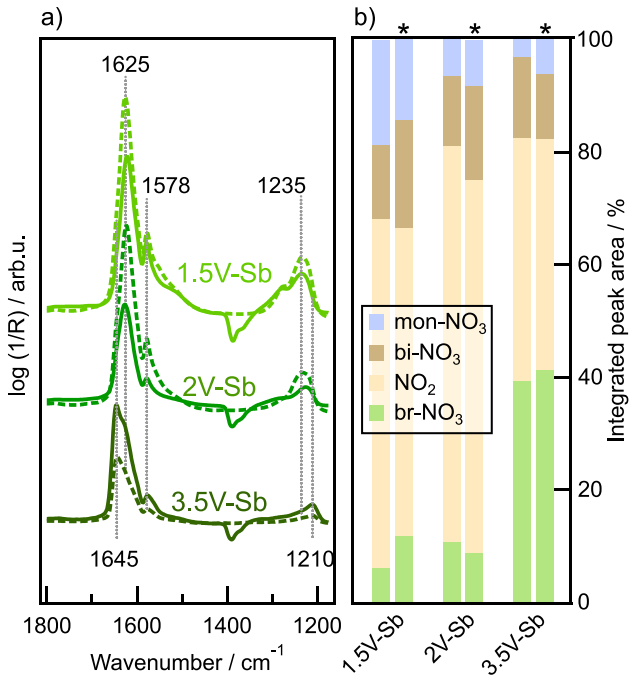

Fig. 6. DRIFT spectra (left) and relative abundance of NO_x species (right) of the V-Sb/TiO_2 catalyst with a different vanadium loading before (solid line) and after (dashed line, *) aging for the NO adsorption at room temperature.

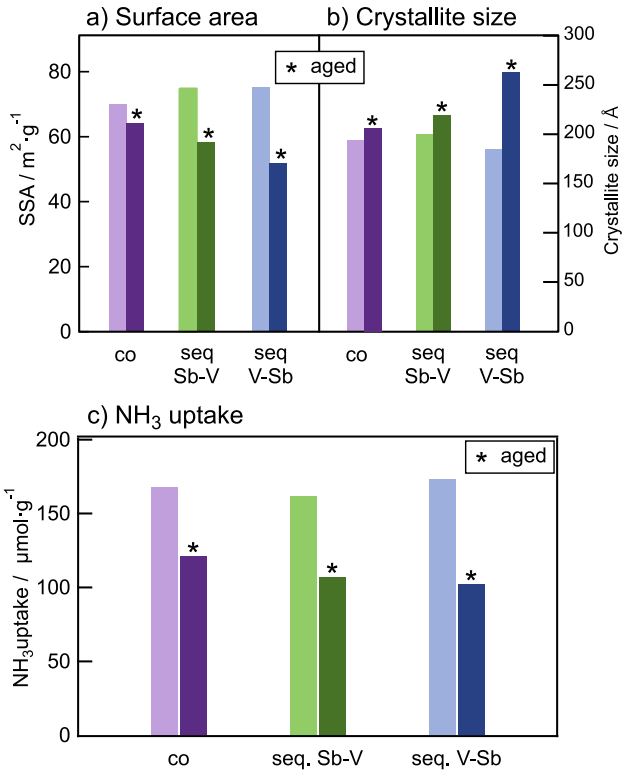

Fig. 7. Comparison of (a) specific surface area, (b) crystallite size, and (c) NH_3 uptake based on NH_3-TPD measurements for the catalysts, prepared *via* co and sequential impregnation, before and after (*) aging.

main band at 1645 cm^{-1} and also confirmed by the respective split vibration at 1210 cm^{-1}. Notably, the overall intensity of the adsorption bands increases on 1.5V-Sb and 2V-Sb after aging. The result of the peak decomposition (Fig. 6b) reveals that the overall ratio of the surface species is only marginally affected by the aging procedure. NO_2 is the dominant species on 1.5V-Sb and 2V-Sb followed by bidentate and monodentate nitrates. With a higher vanadium loading (3.5V-Sb), the bridged nitrates and NO_2 are represented at equal shares. The results of peak decomposition suggest that the addition of antimony affects the ratio of formed NO_x species on the surface. The larger proportion of adsorbed NO_2 on Sb modified catalysts suggest an increased availability and/or oxidation capacity of surface oxygen species that form these NO_2 ad-species rather than nitrate species. This speculation can explain the improved low-temperature SCR activity over the Sb-modified catalysts shown in Fig. 4a. Here, the Sb content was kept constant while the V loading was varied. To further investigate the effect of V/Sb ratio on SCR activity a systematic variation of Sb content for different V loadings would be required. Although it would be interesting to find out the relationship between the nitrates species and the catalytic SCR activity, this is beyond the present scope. The results, however, encourage future detailed studies where, for example, modulation excitation spectroscopy experiments may provide information about active and spectator species *via* phase-sensitive detection analysis [44,45].

3.3. Influence of preparation sequence

In order to investigate the interaction of vanadium oxide, antimony and the titania support, the influence of the preparation sequence was systematically altered. Samples were prepared with an equimolar amount of vanadium and antimony, *via* co-impregnation and sequential impregnation with one compound impregnated on the support first, respectively. When vanadium is added first, the sample was labeled 'seq V-Sb', and vice versa. The target vanadium loading was 2.3 wt% and 5.6 wt% antimony, respectively.

The co-impregnated catalyst (co) exhibits a specific surface area of 70 $m^2\,g^{-1}$, which decreases to 64 $m^2\,g^{-1}$ (−8%) after the aging procedure (Fig. 7a). In comparison, both sequentially impregnated catalysts in fresh state exhibit a higher surface area of 74 $m^2\,g^{-1}$ (seq Sb-V) and 75 $m^2\,g^{-1}$ (seq V-Sb), indicating that the vanadium and antimony preferably interact with each other, thus occupying less TiO_2 sites. After the aging procedure, the catalyst with vanadium added first (seq V-Sb) shows the highest loss in surface area of −31% (75 to 52 $m^2\,g^{-1}$). It is known that vanadium promotes the TiO_2 particle growth [26,27]. As all titania sites are available during the first impregnation, i.e., vanadium in the case of the 'seq V-Sb' catalyst, this reduction is likely due to a larger interface between vanadium and titania for this sample.

Table 2
Specific surface area (SSA) and NH_3 uptake based on NH_3-TPD experiments for the catalysts prepared *via* co and sequential impregnation.

Sample	SSA/$m^2\,g^{-1}$	NH_3 uptake/μ mol g^{-1}
V-Sb co	70	168
V-Sb co aged	64	121
Sb-V seq	74	162
Sb-V seq aged	58	107
V-Sb seq	75	173
V-Sb seq aged	52	102

Further analysis of the anatase diffraction patterns confirm that the crystallite size of 'seq V-Sb' increase the most after the aging procedure (Fig. 7b). Notably, the co-impregnated catalyst maintains the SSA to the greatest extent (70 to 64 $m^2\,g^{-1}$, -8%) while minimizing the growth in crystallite size. The comparison of the determined NH_3 uptake denotes the same trends as for the surface area, revealing a smallest relative decrease for the co-impregnated sample, while the 'seq V-Sb' decreases the most (Fig. 7c). These results are summarized in Table 2.

The analysis of the XRD patterns (Fig. 8a) confirms the previous findings. The co-impregnated catalysts reveals only TiO_2-anatase signatures before and after the aging procedure. On the contrary, both sequentially impregnated catalysts show signatures related to rutile TiO_2 after aging, with more pronounced signatures for the 'seq V-Sb'

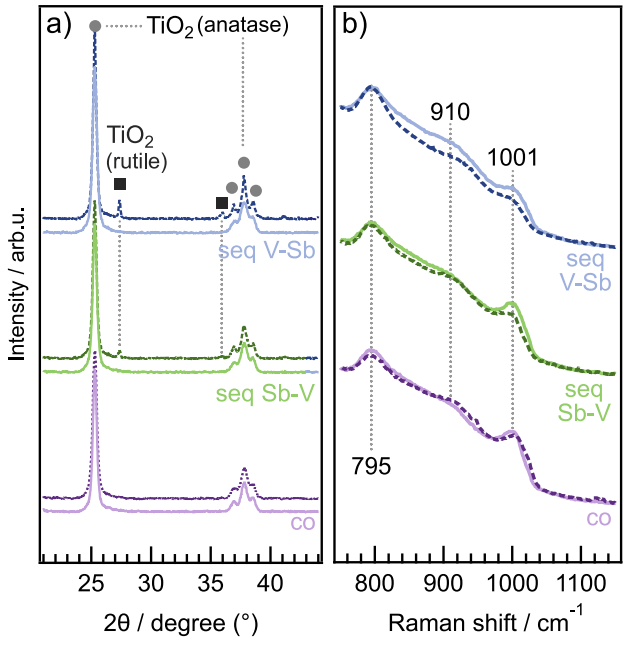

Fig. 8. (a) Background subtracted XRD patterns and (b) Raman spectra (λ = 532 nm) of the V-Sb/TiO_2 catalyst prepared *via* different impregnation procedures before (solid line) and after (dashed) (line) aging under ambient conditions.

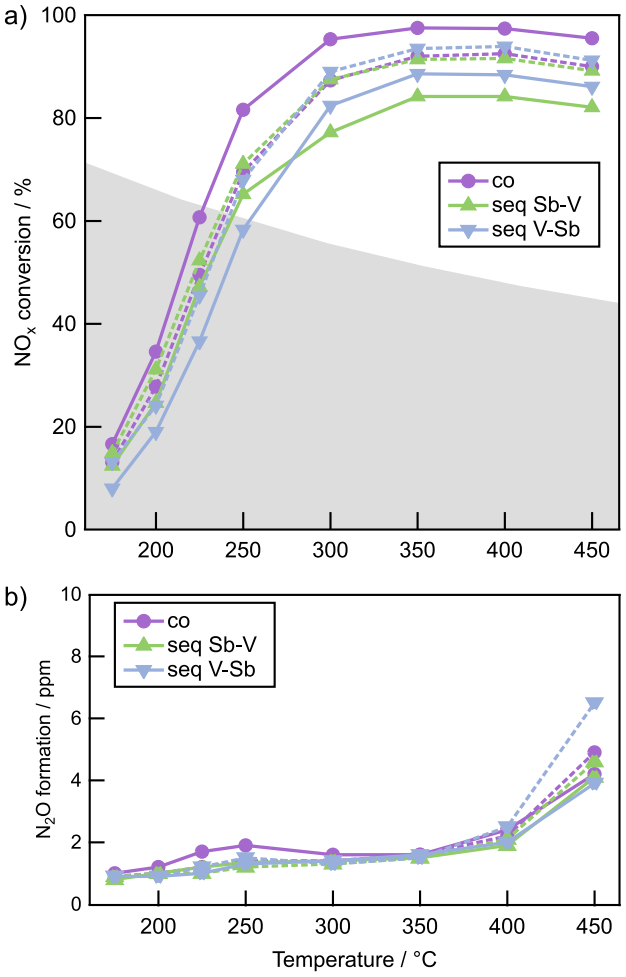

Fig. 9. NO_x conversion of catalysts, prepared *via* co and sequential impregnation, before (solid line) and after (dashed line) aging. The shaded area shows the region where the reaction is kinetically controlled, see SI for mass transfer analysis. Reaction conditions: 525 ppm NH_3, 500 ppm NO, 300 ppm CO, 3% CO_2, 10% O_2, 5% H_2O in Ar/N_2 balance with a GHSV = 60,000 h^{-1}.

catalyst. The Raman spectra of the catalysts (Fig. 8b) reveal features around 910 and 1001 cm^{-1}. Thus the samples predominately contain polymerized VO_x species [39]. The 'co'-impregnated and 'seq Sb-V' catalysts show a higher intensity for the feature at 1001 cm^{-1}. This suggests a higher degree of polymerized VO_x species than on the 'seq V-Sb' catalyst. Since vanadium is added first, the particles can evenly distribute on the available titania sites. After the aging procedure, the spectra reveal minor alterations and therefore suggest that the preparation method does not affect the thermal stability of the VO_x species upon thermal stress.

Fig. 9 shows the steady-state NO_x conversion and N_2O formation as a function of temperature for the fresh and aged catalysts. The fresh co-impregnated catalyst shows the overall highest NO_x conversion across all temperatures. When comparing the sequentially impregnated catalysts, the catalyst with antimony added first ('seq. Sb-V') achieves higher NO_x conversions up to temperatures of 250 °C, while at higher temperatures (≥300 °C) the 'seq V-Sb' catalyst reveals a better performance. After the aging procedure, the NO_x conversion over the co-impregnated catalyst decreases, while both sequentially impregnated catalysts show an increased performance. Notably, the NO_x conversion of all catalysts is similar after aging. The apparent activation energy for the sequentially impregnated catalysts is different for the fresh catalysts but very similar for the aged catalysts (SI, Fig. S10). This supports the interpretation that the aging transforms their surfaces to a similar state and thus they show the same catalytic behavior after aging. Again, the apparent activation energy is similar for the vanadium only catalysts and the antimony modified ones suggesting that the improved low temperature SCR activity for the Sb modified catalysts is a matter of increased availability of active surface oxygen species.

With respect to N_2O formation, the fresh catalysts reveal values between 0.9 to 2 ppm until 350 °C, and reach a level of 4.0 ppm at 450 °C. After aging, the N_2O formation is still moderate for low- to mid-temperatures. At 450 °C, the 'seq V-Sb' catalyst reaches 6.5 ppm N_2O, which is significantly higher in comparison to the other catalysts (4.9, 4.6 ppm)

In order to study alterations on the surface of the catalysts in detail, the ammonia adsorption was monitored *via in situ* DRIFTS (Fig. 10). Based on the previous assignment (Table 1), the suppressed bands of isolated Sb-OH (3695 cm^{-1}), vanadium hydroxyl groups (3650–35 cm^{-1}) and bridged hydroxyls (3622–04 cm^{-1}) are observed. The OH bands of the co-impregnated and 'seq V-Sb' catalyst appear rather similar, while 'seq Sb-V' reveals a higher ratio of isolated Sb-OH (3695 cm^{-1}). The intensity of the V-OH and V-(OH)-V bands is increased, suggesting that more V sites are available after the aging procedure. Alongside with that, the bands for the bridged OH groups decrease while the Sb-OH intensity is maintained, indicating a segregation of vanadium and antimony species. Only the 'seq Sb-V' catalyst reveals a distinct decline of the of Sb-OH band (3695 cm^{-1}). In the N-H vibrational region, the resulting absorption bands of ammonia adsorbed on Lewis (1605 cm^{-1}) and Brønsted (1470–35 cm^{-1}) acid sites are similar across all catalysts. The weak sulfate signal (around 1360 cm^{-1}) for co-impregnated catalysts indicates a high coverage of the support, as stated previously. After aging, the intensity of the Lewis acid band is increased for all catalysts. The Brønsted acid band is slightly decreased for the co-impregnated catalysts, while 'seq V-Sb' sample reveals a marked decline in intensity.

It is important to note that after the aging procedure, the resulting ammonia adsorption spectra of all catalysts resemble each other showing similar intensities of the respective infrared bands, which also correlates with the converged NO_x conversion.

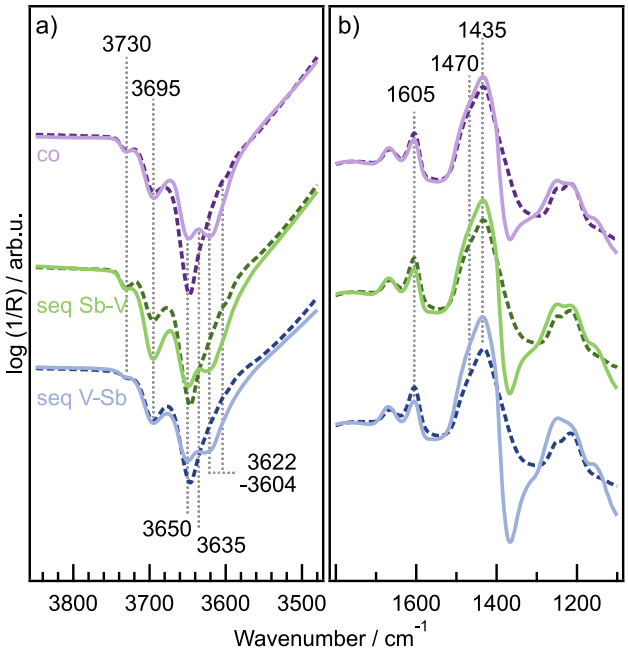

Fig. 10. DRIFT spectra of the V-Sb/TiO_2 catalyst prepared *via* different impregnation procedures before (solid line) and after (dashed line) aging for the NH_3 adsorption at room temperature. (a) ν(O-H) region and (b) δ(N-H) deformation modes of ammonia.

3.4. Consequences of the antimony modification for deactivation mechanisms

A visualization of the interpreted results is displayed in Fig. 11, with the aim to clarify how the modification with antimony suppresses the catalyst deactivation and which mechanisms are involved. During the aging procedure of titania-supported vanadium oxides (VO_x/TiO_2), the TiO_2 and VO_x phases undergo different changes and some mechanisms are particularly controlling. Commonly, thermal aging involves sintering of the anatase TiO_2 particles, eventually accompanied by an anatase-to-rutile phase transformation, leading to a significant loss of the specific surface area which is directly linked to the particle growth. The presence of vanadium oxides on titania enhances those processes, and the effect correlates to the added amount or rather surface density of the vanadium oxides [26,46]. The decreased available surface area for the dispersed phase affects the VO_x species, as those may undergo aggregation, forming higher polymerized VO_x species, and in some cases forming crystalline V_2O_5, eventually also leading to pore clogging [3]. Crystalline V_2O_5 particles promote side reactions such as ammonia oxidization and N_2O formation, ultimately resulting in an overall decreased catalytic performance [26,47] as specified for the reference catalyst in Fig. 4.

The modification with antimony proves a stabilizing effect on both the TiO_2 support and the VO_x species which is represented in a maintained specific surface area along with a minimized particle size growth after the aging procedure. The characterization of the catalysts shows that the absolute majority of the titania sites are covered by the vanadium and antimony oxides, which in turn counteracts the anatase sintering as well as VO_x species agglomeration (except for 3.5V-Sb).

4. Conclusions

In this study, the effect of the modification of titania supported VO_x catalysts with antimony oxide has been investigated as well as the effect of thermal aging. We demonstrate that the addition of antimony has proven to hold an inherent SCR activity and to stabilize the anatase phase of TiO_2 including a minimized particle size growth. For the Sb-modified VO_x/TiO_2 catalysts, the addition of antimony does not enhance the overall acidity in regard to the total NH_3 uptake. The molar ratio of V and Sb appears to be crucial for the catalytic performance after thermal stress, as only 2V-Sb with a molar ratio of 1.2 V/Sb shows an increased NO_x conversion after the aging procedure. The increased performance may be related to enhanced redox properties due to interaction of vanadium and antimony species. Further, the *in situ* DRIFT spectra suggest the exposure of additional vanadium sites, as indicated by an increased intensity of V-OH/V-(OH)-V groups. Further, the N_2O formation is much lower when the catalysts are modified with antimony in comparison to the reference. The molar ratio of 2 V/Sb is detrimental on the basis of a significant loss of surface area, the formation of V_2O_5, and an increased N_2O formation while maintaining a high activity. In addition, we find an important effect of the impregnation method for the catalyst in fresh state, with an overall higher performance when the two compounds are added *via* co-impregnation. When V is added first, it is more likely to affect the TiO_2-anatase phase negatively, implied by a loss of surface area accompanied by a transformation from anatase to rutile.

CRediT authorship contribution statement

Alexander Nellessen: Writing – original draft, Visualization, Methodology, Investigation, Formal analysis, Data curation. **Roberta Villamaina:** Project administration, Formal analysis, Data curation. **Andreas Schaefer:** Writing – review & editing, Supervision, Investigation, Formal analysis, Data curation. **Agnes Raj:** Project administration, Formal analysis, Data curation, Conceptualization. **Andrew Newman:** Conceptualization. **Anna Martinelli:** Writing – review & editing, Supervision, Investigation, Formal analysis. **Per-Anders Carlsson:** Writing – review & editing, Supervision, Methodology, Investigation, Funding acquisition, Formal analysis, Conceptualization.

Declaration of competing interest

The authors declare the following financial interests/personal relationships which may be considered as potential competing interests: Per-Anders Carlsson reports financial support was provided by Energimyndigheten. Per-Anders Carlsson reports financial support was provided by Swedish Research Council. If there are other authors, they declare that they have no known competing financial interests or personal relationships that could have appeared to influence the work reported in this paper.

Acknowledgments

This work was financially supported by the Swedish Energy Agency through the FFI program “Ultra-efficient recyclable De-NOx catalysts for biofuel and hybrid powertrains” (No. 51318-1), the Swedish Research Council through the project “Infrared Spectroscopy in Time and Space” (Dnr. 2019-05528) and the Competence Centre for Catalysis, which is hosted by Chalmers University of Technology and financially supported by the Swedish Energy Agency and the member companies AB Volvo, ECAPS AB, Johnson Matthey Plc, Perstorp AB, Preem AB, Scania CV AB, Umicore AG & Co. KG. Parts of this work were performed at the Chalmers Material Analysis Laboratory, CMAL.

Data availability

Data will be made available on request.

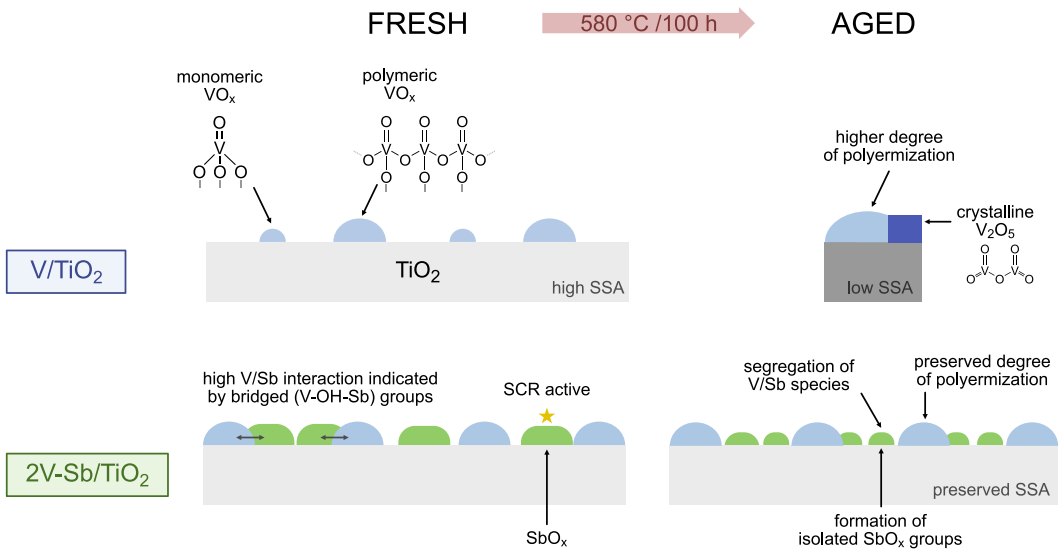

Fig. 11. Schematic illustration of the consequences of the aging procedure and the deactivation mechanisms on the Sb-modified catalyst with a V loading of 2 wt% (2V-Sb/TiO_2) and the reference catalyst.

References

[1] J.K. Lai, I.E. Wachs, A perspective on the selective catalytic reduction (SCR) of NO with NH_3 by supported V_2O_5-WO_3/TiO_2 catalysts, ACS Catal. 8 (7) (2018) 6537–6551, http://dx.doi.org/10.1021/acscatal.8b01357.

[2] S.E. Bozbağ, D. Şanlı, B. Özener, G. Hisar, C. Erkey, Development of a model based strategy for catalyst screening to control NO_x and N_2O emissions in $[NH]_3$-SCR process towards Eu7 readiness, J. Environ. Chem. Eng. 11 (3) (2023) 110232, http://dx.doi.org/10.1016/j.jece.2023.110232.

[3] G. Madia, M. Elsener, M. Koebel, F. Raimondi, A. Wokaun, Thermal stability of vanadia-tungsta-titania catalysts in the SCR process, Appl. Catal. B Environ. 39 (2) (2002) 181–190, http://dx.doi.org/10.1016/S0926-3373(02)00099-1.

[4] G. He, Z. Lian, Y. Yu, Y. Yang, K. Liu, X. Shi, Z. Yan, W. Shan, H. He, Polymeric vanadyl species determine the low-temperature activity of V-based catalysts for the SCR of NO_x with NH_3, Sci. Adv. 4 (11) (2018) 1–8, http://dx.doi.org/10.1126/sciadv.aau4637.

[5] N.R. Jaegers, J.-K.K. Lai, Y. He, E. Walter, D.A. Dixon, M. Vasiliu, Y. Chen, C. Wang, M.Y. Hu, K.T. Mueller, I.E. Wachs, Y. Wang, J.Z. Hu, Mechanism by which tungsten oxide promotes the activity of supported V_2O_5/TiO_2 catalysts for NO_x abatement: Structural effects revealed by 51V MAS NMR spectroscopy, Angew. Chem. Int. Ed. 58 (36) (2019) 12739–12746, http://dx.doi.org/10.1002/ange.201904503.

[6] I.E. Wachs, Catalysis science of supported vanadium oxide catalysts, Dalton Trans. 42 (33) (2013) 11762–11769, http://dx.doi.org/10.1039/c3dt50692d.

[7] D.G. Barceloux, D.D. Barceloux, Vanadium, J. Toxicol. Clin. Toxicol. 37 (2) (1999) 265–278, http://dx.doi.org/10.1081/CLT-100102425, PMID: 10382561.

[8] I.E. Wachs, Y. Chen, J.M. Jehng, L.E. Briand, T. Tanaka, Molecular structure and reactivity of the group V metal oxides, Catal. Today 78 (1-4 SPEC.) (2003) 13–24, http://dx.doi.org/10.1016/S0920-5861(02)00337-1.

[9] Vanadium and tungsten release from V-based selective catalytic reduction diesel aftertreatment, Atmos. Environ. 104 (2015) 154–161, http://dx.doi.org/10.1016/j.atmosenv.2014.12.063.

[10] C. Chen, Y. Cao, S. Liu, J. Chen, W. Jia, Review on the latest developments in modified vanadium-titanium-based SCR catalysts, Chin. J. Catal. 39 (8) (2018) 1347–1365, http://dx.doi.org/10.1016/S1872-2067(18)63090-6.

[11] L. Lietti, I. Nova, G. Ramis, L. Dall'Acqua, G. Busca, E. Giamello, P. Forzatti, F. Bregani, Characterization and reactivity of V_2O_5–MoO3/TiO_2 De-NO_x SCR catalysts, J. Catalysis 187 (2) (1999) 419–435, http://dx.doi.org/10.1006/jcat.1999.2603.

[12] D.M. Chapman, G. Fu, S. Augustine, M. Watson, J. Crouse, L. Zavalij, D. Perkins-Banks, New titania materials with improved stability and activity for vanadia-based selective catalytic reduction of NO_x, SAE Int. J. Fuels Lubr. 3 (1) (2010) 643–653, http://dx.doi.org/10.4271/2010-01-1179.

[13] M. Kobayashi, R. Kuma, S. Masaki, N. Sugishima, Tio_2-SiO_2 and V_2O_5/TiO_2-SiO_2 catalyst: Physico-chemical characteristics and catalytic behavior in selective catalytic reduction of NO by NH_3, Appl. Catal. B Environ. 60 (3) (2005) 173–179, http://dx.doi.org/10.1016/j.apcatb.2005.02.030.

[14] Y. Pan, W. Zhao, Q. Zhong, W. Cai, H. Li, Promotional effect of Si-doped V_2O_5/TiO_2 for selective catalytic reduction of NO_x by NH_3, J. Environ. Sci. 25 (8) (2013) 1703–1711, http://dx.doi.org/10.1016/S1001-0742(12)60181-8.

[15] A.M. Beale, I. Lezcano-Gonzalez, T. Maunula, R.G. Palgrave, Development and characterization of thermally stable supported V–W–TiO_2 catalysts for mobile NH_3–SCR applications, Catal. Struct. React. 1 (1) (2015) 25–34, http://dx.doi.org/10.1179/2055075814Y.0000000005.

[16] X. Du, X. Gao, Y. Fu, F. Gao, Z. Luo, K. Cen, The co-effect of sb and nb on the SCR performance of the $V_2O_5TiO_2$ catalyst, J. Colloid Interface Sci. 368 (1) (2012) 406–412, http://dx.doi.org/10.1016/j.jcis.2011.11.026.

[17] D.W. Kwon, D.H. Kim, S.C. Hong, Promotional effect of antimony on the selective catalytic reduction NO with NH_3 over V-Sb/Ti catalyst, Environ. Technol. (United Kingdom) 40 (19) (2019) 2577–2587, http://dx.doi.org/10.1080/09593330.2018.1491632.

[18] Z. Liu, S. Zhang, J. Li, J. Zhu, L. Ma, Novel V_2O_5-CeO_2/TiO_2 catalyst with low vanadium loading for the selective catalytic reduction of NO_x by NH_3, Appl. Catal. B Environ. 158–159 (2014) 11–19, http://dx.doi.org/10.1016/j.apcatb.2014.03.049.

[19] I.E. Wachs, J.M. Jehng, G. Deo, H. Hu, N. Arora, Redox properties of niobium oxide catalysts, Catal. Today 28 (1–2) (1996) 199–205, http://dx.doi.org/10.1016/0920-5861(95)00229-4.

[20] J.H. Shin, G.R. Choi, S.C. Hong, Vanadium catalyst based on a tungsten trioxide structure modified with antimony in NH_3-selective catalytic reduction for improved low-temperature activity, Appl. Surf. Sci. 574 (2022) 151571, http://dx.doi.org/10.1016/j.apsusc.2021.151571.

[21] Y.E. Jeong, P.A. Kumar, H.P. Ha, K. young Lee, Highly active Sb–V–CeO_2/TiO_2 catalyst under low sulfur for NH_3-SCR at low temperature, Catal. Lett. 147 (2) (2017) 428–441, http://dx.doi.org/10.1007/s10562-016-1951-y.

[22] Y.E. Jeong, P.A. Kumar, D.T. Huong, H.P. Ha, K.Y. Lee, In situ-DRIFTS study of Sb–V–CeO_2/TiO_2 catalyst under standard and fast NH_3-SCR conditions, Top. Catal. 60 (9–11) (2017) 755–762, http://dx.doi.org/10.1007/s11244-017-0784-2.

[23] Y.E. Jeong, P.A. Kumar, H.P. Ha, K. young Lee, Effect of hydrothermal aging on NO_x reduction performance for Sb–V–CeO_2/TiO_2 catalyst, Res. Chem. Intermed. 44 (11) (2018) 6803–6829, http://dx.doi.org/10.1007/s11164-018-3523-9.

[24] P.A. Kumar, Y.E. Jeong, H.P. Ha, Low temperature NH_3-SCR activity enhancement of antimony promoted vanadia-ceria catalyst, Catal. Today 293–294 (2017) 61–72, http://dx.doi.org/10.1016/j.cattod.2016.11.054.

[25] Y.K. Bae, T.W. Kim, J.R. Kim, Y. Kim, K.S. Ha, H.J. Chae, Enhanced SO_2 tolerance of V_2O_5-Sb_2O_3/TiO_2 catalyst for NO reduction with co-use of ammonia and liquid ammonium nitrate, J. Ind. Eng. Chem. 96 (2021) 277–283, http://dx.doi.org/10.1016/j.jiec.2021.01.029.

[26] A. Nellessen, A. Schaefer, A. Martinelli, A. Raj, A. Newman, P.-A. Carlsson, Impact of vanadium loading and thermal aging on the surface properties of titania supported vanadium oxide, J. Phys. Chem. C 128 (7) (2024) 2894–2908, http://dx.doi.org/10.1021/acs.jpcc.3c08081.

[27] A. Kubacka, A. Iglesias-Juez, M. di Michiel, A.I. Becerro, M. Fernández-García, Morphological and structural behavior of TiO_2 nanoparticles in the presence of WO_3: Crystallization of the oxide composite system, Phys. Chem. Chem. Phys. 16 (36) (2014) 19540–19549, http://dx.doi.org/10.1039/c4cp02181a.

[28] H. Kamata, H. Ohara, K. Takahashi, A. Yukimura, Y. Seo, SO_2 oxidation over the V_2O_5/TiO_2 SCR catalyst, Catal. Lett. 73 (1) (2001) 79–83, http://dx.doi.org/10.1023/A:1009065030750.

[29] O. Saur, M. Bensitel, A. Saad, J. Lavalley, C.P. Tripp, B. Morrow, The structure and stability of sulfated alumina and titania, J. Catalysis 99 (1) (1986) 104–110, http://dx.doi.org/10.1016/0021-9517(86)90203-4.

[30] F. Giraud, C. Geantet, N. Guilhaume, S. Loridant, S. Gros, L. Porcheron, M. Kanniche, D. Bianchi, Experimental microkinetic approach of De-NO_x by NH_3 on $V_2O_5/WO_3/TiO_2$ catalysts. 2. Impact of superficial sulfate and/or V_xO_y groups on the heats of adsorption of adsorbed NH_3 species, J. Phys. Chem. C 118 (29) (2014) 15677–15692, http://dx.doi.org/10.1021/jp502583k.

[31] R.A. Eppler, Effect of antimony oxide on the anatase-rutile transformation in titanium dioxide, J. Am. Ceram. Soc. 70 (4) (1987) C–64–C–66, http://dx.doi.org/10.1111/j.1151-2916.1987.tb04985.x.

[32] T.Z. Srnak, J.A. Dumesic, B.S. Clausen, E. Törnqvist, N.Y. Topsøe, Temperature-programmed desorption/reaction and in situ spectroscopic studies of vanadia/titania for catalytic reduction of nitric oxide, J. Catalysis 135 (1) (1992) 246–262, http://dx.doi.org/10.1016/0021-9517(92)90283-N.

[33] G. Busca, L. Lietti, G. Ramis, F. Berti, Chemical and mechanistic aspects of the selective catalytic reduction of NO(x) by ammonia over oxide catalysts: A review, Appl. Catal. B Environ. 18 (1–2) (1998) 1–36, http://dx.doi.org/10.1016/S0926-3373(98)00040-X.

[34] M. Koebel, M. Elsener, M. Kleemann, Urea-SCR: a promising technique to reduce NO_x emissions from automotive diesel engines, Catal. Today 59 (3) (2000) 335–345, http://dx.doi.org/10.1016/S0920-5861(00)00299-6.

[35] S. Djerad, L. Tifouti, M. Crocoll, W. Weisweiler, Effect of vanadia and tungsten loadings on the physical and chemical characteristics of V_2O_5-WO_3/TiO_2 catalysts, J. Mol. Catal. A: Chemical 208 (2004) 257–265, http://dx.doi.org/10.1016/j.molcata.2003.07.016.

[36] I.R. Beattie, T.R. Gilson, Oxide phonon spectra, J. Chem. Soc. A Inorg. Phys. Theor. Chem. (1969) 2322–2327, http://dx.doi.org/10.1039/J19690002322.

[37] J.-K. Lai, N.R. Jaegers, B.M. Lis, M. Guo, M.E. Ford, E. Walter, Y. Wang, J.Z. Hu, I.E. Wachs, Structure-activity relationships of hydrothermally aged titania-supported vanadium-tungsten oxide catalysts for SCR of NO_x emissions with NH_3, ACS Catal. 11 (19) (2021) 12096–12111, http://dx.doi.org/10.1021/acscatal.1c02130.

[38] M.A. Vuurman, I.E. Wachs, A.M. Hirt, Structural determination of supported V_2O_5-WO_3/TiO_2 catalysts by in situ Raman spectroscopy and X-ray photoelectron spectroscopy, J. Phys. Chem. 95 (24) (1991) 9928–9937, http://dx.doi.org/10.1021/j100177a059.

[39] G.T. Went, L.-J. Leu, A.T. Bell, Quantitative structural analysis of dispersed vanadia species in TiO_2(anatase)-supported V_2O_5, J. Catalysis 134 (2) (1992) 479–491, http://dx.doi.org/10.1016/0021-9517(92)90336-G.

[40] N.Y. Topsøe, J.A. Dumesic, H. Topsøe, Vanadia-titania catalysts for selective catalytic reduction of nitric-oxide by ammonia. II. Studies of active sites and formulation of catalytic cycles, J. Catalysis 151 (1) (1995) 241–252, http://dx.doi.org/10.1006/jcat.1995.1025.

[41] A. Marberger, D. Ferri, M. Elsener, O. Kröcher, The significance of lewis acid sites for the selective catalytic reduction of nitric oxide on vanadium-based catalysts, Angew. Chem. Int. Ed. 55 (39) (2016) 11989–11994, http://dx.doi.org/10.1002/anie.201605397.

[42] L. Lietti, J. Svachula, P. Forzatti, G. Busca, G. Ramis, F. Bregani, Surface and catalytic properties of vanadia-titania and tungsta-titania systems in the selective catalytic reduction of nitrogen oxides, Catal. Today 17 (1993) 131–140, http://dx.doi.org/10.1016/0920-5861(93)80016-T.

[43] L. Lietti, P. Forzatti, Temperature programmed desorption/reaction of ammonia over V2o5/TiO2 De-NOxing catalysts, J. Catalysis 147 (1993) 241–249, http://dx.doi.org/10.1006/jcat.1994.1135.

[44] P. Müller, I. Hermans, Applications of modulation excitation spectroscopy in heterogeneous catalysis, Ind. Eng. Chem. Res. 56 (45) (2017) 1123–1136, http://dx.doi.org/10.1021/acs.iecr.6b04855.

[45] F. Hemmingsson, A. Schaefer, M. Skoglundh, P.-A. Carlsson, CO2 methanation over Rh/CeO2 studied with infrared modulation excitation spectroscopy and phase sensitive detection, Catalysts 10 (6) (2020) 601.

[46] G. Oliveri, G. Ramis, G. Busca, V. Sanchez Escribanob, Thermal stability of vanadia-titania catalysts, J. Mater. Chem. 3 (12) (1993) 1239–1249, http://dx.doi.org/10.1039/JM9930301239.

[47] J.M. Won, M.S. Kim, S.C. Hong, The cause of deactivation of VO_x/TiO_2 catalyst by thermal effect and the role of tungsten addition, Chem. Eng. Sci. 229 (2021) 116068, http://dx.doi.org/10.1016/j.ces.2020.116068.